

# Enhanced Mapping of High-resolution Lunar Elemental Ratios: Lunar Compositional Analysis from X-Ray Fluorescence Data of Chandrayaan 2

Team 30

---

## Abstract

The Moon is the most significant celestial object known to mankind and has been studied by astronomers over centuries. In the past few decades, multiple missions have been carried out to study detailed lunar features to know about its formation and evolution. Studying lunar elemental composition is an important aspect of knowing its geochemistry and morphology over the past 4.5 billion years. Apollo missions being the first to collect lunar samples set significant milestones by setting a platform for our understanding of lunar evolution. Various missions enhanced our knowledge by studying the lunar crust's composition in different spectral ranges. X-ray fluorescence spectroscopy (XRF) provides an independent method to derive elemental composition by offering higher sensitivity to lighter elements. C1XS and CLASS with their pioneering high-resolution data provided significant insights to deepen our understanding of lunar processes. The study is focused on mapping elemental ratios with respect to Si from an extensive CLASS XRF dataset over the past 5 years with the highest resolution and coverage to date. Studying elemental ratio maps of Mg/Si, Al/Si and other major lunar elements with respect to Si over lunar regions gives us insights into the evolution of the region over time and also provides insights into volcanism in that region in the past. This gives us a keen understanding to further study individual regions and plan future missions to study those regions.

**Keywords:** Chandrayaan 2, XRF, CLASS, Lunar elemental composition, Elemental ratios.

---

## 1. Introduction

Studying the geochemical composition of the Lunar surface gives many clues about its evolution. Following the catastrophic impact Earth underwent 4.5 billion years ago, the Earth moved on with hardly any memory. The Moon cooled down and formed a crust, mantle, and core, and it stood as a canvas to mark early solar system events. Since the Moon does not have any active geological process (e.g. wind, river erosion, etc), it preserves the records of billions of year-old events. Studying the elemental composition of the lunar crust can give us significant insights into the history of the Earth and the Moon, enhance our understanding of theories of its formation, and open up doors to study evolution processes accurately. Multiple missions have been carried out since the 1950s, and lunar geo-chemistry has been deciphered through various missions focusing on studies in near IR, X-ray, gamma-ray, UV, radar, neutron, and even through direct samples from Apollo. With the addition of significant insights from each mission exploration, researchers have continuously updated our understanding of lunar formation and evolution, with Chandrayaan 2 being the pioneer

in detailed X-ray fluorescence exploration.

### 1.1. Key missions on XRF study of lunar Surface

**Apollo 15 and 16** (1969-1972) were the first missions to study lunar geochemistry, having coverage of 10% area with remote sensing X-ray fluorescence spectroscopy experiment to obtain empirical values of Mg and Al concentration relative to Si. This was the first mission to understand the composition of the bulk crust of the lunar surface and identify between Mare and Highland. [Gloude-mans et al. \(2021\)](#) provides the most recent analysis of these missions.

**SMART-1** (2003-2004) later refined the lunar crust compositional understandings using the demonstration of a compact imaging X-ray spectrometer (D-CIXS) instrument with 24 miniaturized X-ray detectors. Mapping the distribution of Mg on the lunar surface was a high scientific priority, accompanied by an X-ray Solar Monitor (XSM) for monitoring input Solar X-ray flux. The first successful detection of K-alpha lines for Ti, Ca, and Fe added to primary diagnostics of mare basalt petrogenesis improvised characterization of areas of basaltic composition and highland regions, whereas radiation damage left the

low energy lines of Mg, Al, and Si unresolved and deconvolving individual contributions to the spectrum from these lines was challenging ([Swinyard et al. \(2009\)](#)).

**SELENE-Kaguya** (2007-2008) had achieved global coverage of major elements of Mg, Al, and Si, except at poles and Ca, Ti, and Fe at the scale of basins. X-ray spectrometry instruments consisted of instrument that consisted CCD-based main detector with a direct monitor of Solar X-ray along with XRF calibrator. The mission also investigated the physical processes of lunar X-ray illumination during the Night-time, which occurred due to solar wind particles, cosmic rays, and natural radioactivity. It also investigated regional variation of surface roughness as a result of particle size effect on XRF but damage suffered from radiation prevented useful measurements ([Okada et al. \(2010\)](#)).

**Chandrayaan 1** (2008-2009) pioneered lunar XRF data of the best spectral and spatial resolution to date. The Chandrayaan 1 X-ray Spectrometer (C1XS) instrument, mounted with XSM, performed high-resolution mapping of Mg, Al, Si, Ca, and Fe for the Highland region for the Southern nearside of the Moon. The methodology implemented helped find abundances of these elements with limited consistency over regions studied during times of solar flares powerful enough to simulate detectable surface fluorescence in a short 9-month mission ([Narendranath et al. \(2011\)](#)).

**Chang'E-2** (2010-2012) was the first to globally map Mg/Si and Al/Si distribution on the lunar surface from Chang-E 2 X-ray spectrometer (CE2XRS), integrated with XSM and also refined its findings from Chang'E 1 mission to enhance our understanding on lunar surface material evolution. However, Si-PIN detectors with an area of 4 cm<sup>2</sup> resulted in poor spectral resolution ([Ban et al. \(2014\)](#)).

**Chandrayaan 2** (2019-present) came up with the most sophisticated instrument to date; Chandrayaan-2 Large Area Soft X-ray Spectrometer (CLASS) which consists of sixteen swept charge devices (SCDs) aims to obtain the best spatial and spectral resolution. Integrated XSM measures the solar spectrum simultaneously. All specifications together contribute to CLASS's ability to measure the X-ray spectrum in the energy range 0.5eV to 20eV, providing the most insights about major lunar crust's elements, namely O, Mg, Al, Si, Ca, Ti, and Fe; and determining elemental abundances on Highland and Mare region.

**CLASS significance** - With a geometric area of 64cm<sup>2</sup> built up by sixteen (SCDs) arranged as four quads, when

the door is closed, the radioactive sources illuminate the SCDs and are used for calibration. Gold-coated copper collimators with a field of view of each SCD as 7° × 7° Full Width at Half Maximum (FWHM), which translates to 12.5km×12.5km footprint at the 100km altitude providing the best spatial resolution to date and is successfully detecting maximum no of elements done by any lunar mission ([Pillai et al. \(2021\)](#)).

## 2. Objective

Objective focuses on mapping the elemental composition of the lunar crust for major lunar elements: O, Mg, Al, Si, Ca, Ti, Cr, and Fe, which showed detectable peaks in XRF. The Orbiter has a projected lifespan of 7 years. In its exploration since 2019, with an orbital period of 2 hours, it has achieved maximum global coverage for major elements during periods of significant solar activities. Elemental composition for these elements is mapped in terms of ratios, which eliminates the effects of Solar flare intensity, solar zenith angle, and related parameters affecting XRF to predict elemental abundances. Using ratios will mitigate these uncertainties and retain the elemental composition's accuracy. Variation in elemental composition over regions helps us to determine compositional groups for different terrains on the Moon, like Mare, and Highland. A high spatial resolution of 12.5km×12.5km can provide us with the most accurate surface data to determine geochemical composition. Increasing resolution by subpixel resolution techniques will refine our compositional maps to provide detailed ideas about variations on a few km scales. With the extensive data from the most prolonged lunar mission, the study focuses on building a dynamic algorithm that could provide high-resolution compositional maps from past and incoming data and decipher meaningful inferences about surface composition from the elemental ratio maps generated.

## 3. Methodology

### 3.1. Data Collection

#### 3.1.1. CLASS

The primary data of our research interest is Chandrayaan-2 Large Area Soft X-ray Spectrometer(CLASS) data, which gives us a dataset in which a particular file is XRF spectrum captured by CLASS instrument over a patch of 12.5km × 12.5km from the altitude of 100 km. This serves as our basis for elemental composition analysis at a particular location. Files with solar

phase angles less than 90° are considered for elemental ratios and files with solar phase angles more than 90° are regarded for background analysis.

### 3.1.2. XSM

The data from the X-ray Solar Monitor has .pha files of the solar continuum at a particular TIMESTAMP. These .pha files are used for normalizing relative elemental abundances from XRF spectra to get ratios of actual abundances.

### 3.2. Background removal

Lunar background refers to radiation from Galactic cosmic rays, solar winds, and occasionally solar energetic particles which add up to surface elemental XRF spectra and even through Geotail. This background needs to be removed and is even over the whole lunar surface at a particular time instant. This background can be clearly detected in CLASS's Night-time observations when XRF due to solar flares is obstructed. The phase angle of the orbiter gives us details about the position of the orbiter on the Moon with respect to the sun and gives us insights about its night-time. The phase angle of more than 90° defines the positioning of the orbiter on the night side. The orbiter operates for 5 minutes at night time when it collects background data, which is termed night-side background data [Pillai et al. \(2021\)](#).

### Geotail interference

The Moon passes through the Geotail of Earth 6 days in its orbit. CLASS observed a surge in background count intensity these days. Particles emitted in Geotail are detected by CLASS which are not part of lunar elemental emission and hence need to be removed as background. A peak at Al and Fe was seen in the background corresponding to these emissions [Nishida et al. \(1992\)](#).

Surface temperature gradient causes a gradual decrease in spectral peak intensity for solar phase angles from 90° to 180°, showing a relatively significant gradient near 90° and less gradient for angles away. The farther angles have nearly the same peak intensities. Our actual background to be subtracted should be consistent with any location on the lunar surface at a particular instant. The higher the solar phase angle, the more it will show an accurate night-time background. The most accurate background data will be near a phase angle of 180°. However, empirical studies we conducted showed slight gradience near a phase angle of 90° with a nearly consistent background for phase angles from 90° to 180°. This

observation could be potentially due to the polar orbit of Chandrayaan 2 which has lesser excitation at cold poles. Also, due to limited CLASS data of night-time observation, the threshold solar phase angle for night-time background characterization was taken as 91° (a 1-degree margin is kept to avoid boundary effects). These files are averaged out for a particular orbit to get the background of that orbital revolution. The final background removed file is prepared by subtracting background counts from detected XRF counts corresponding to every channel [Narendranath et al. \(2011\)](#).

### 3.3. Noise reduction and spectral fitting

The original XRF spectrum is interfered by noise induced by electronic noise, detector limitations, or other environmental factors which is removed by the moving average, refined the spectrum by eliminating instantaneous spikes, and smoothed out the spectra.

The spectrum was further refined by the Gaussian fitting technique, which improves spectrum resolution, models elemental peaks, and improves the signal-to-noise ratio (SNR) to give a fine-tuned spectrum. We considered elemental peak when it is 3 standard deviations above the mean, ensuring a 99.7% confidence level for peak detection. This minimizes false peak detection, which can cause weaker peaks generated by Cosmic background and detector noise. This will reduce our coverage but increase our accuracy and is optimum for large datasets which CLASS will generate in its 7 years.

### 3.4. Elemental Peak Identification

The elements of our research interest, being major lunar surface elements and Cr have signature K-alpha peaks at O - 0.52 keV, Mg - 1.25 keV, Al - 1.56 keV, Si - 1.74 keV, Ca - 3.69 keV, Ti - 4.51 keV, Cr - 4.41 keV and Fe - 6.4 keV. The fluctuations due to detection errors were taken into account by defining the threshold of energy range for peak detection. K-alpha and K-beta excitation energy difference increases with atomic number so we can safely neglect K-beta peaks for higher atomic number elements. Lower atomic number elements have **K- $\alpha$**  and **K- $\beta$**  peaks very close but due to the lower **K- $\beta$ /K- $\alpha$**  ratio for lighter elements we can safely neglect **K- $\beta$**  peaks in lower atomic number elements as well for our analysis [Ito et al. \(2023\)](#).

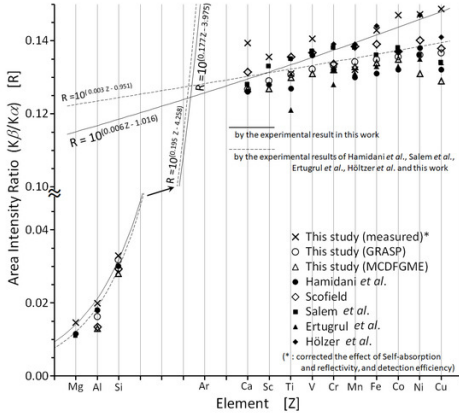


Figure 1:  $K\beta/K\alpha$  for elements

### 3.5. Coverage mapping

Elemental peak detection at various locations is mapped on LROC with the position coordinates of latitude and longitudes of the CLASS file. These coverage maps denotes successful elemental peak detections in the form of patches of  $12.5\text{km} \times 12.5\text{km}$  defining a particular CLASS file. The individual maps are generated for all elements of our interest.

### 3.6. Spectral normalization

The incident solar spectra have different intensities of photons corresponding to different energy values. The excitation of lunar elements is subject to this solar spectrum causing their excitation. This solar spectrum follows behavior similar to power law distribution. The lower intensity of counts in a higher energy range is not necessarily due to a lower abundance of elements corresponding to excitation energy of that energy range but also due to a lower number of photons incident of that energy owing to the power law distribution behavior of solar spectra. Similarly higher intensity of counts in a lower energy range is not necessarily due to a higher abundance of elements corresponding to excitation energy in this energy range but also due to a higher number of photons incident of that energy range from solar spectra. The counts for the abundance that we are getting are with respect to the solar spectrum causing that excitation. Hence to proceed with getting actual relative abundances we divide our processed, background removed, continuum subtracted spectra with solar continuum at that period. This gives us counts for relative abundances with respect to situations when a unit set of photons would have an incident for each energy range. This will give us actual relative abundance provided the incident spectrum would

have the same number of photons incident for each energy range. This will give us the correct relative abundances of elements in particular locations on the lunar surface.

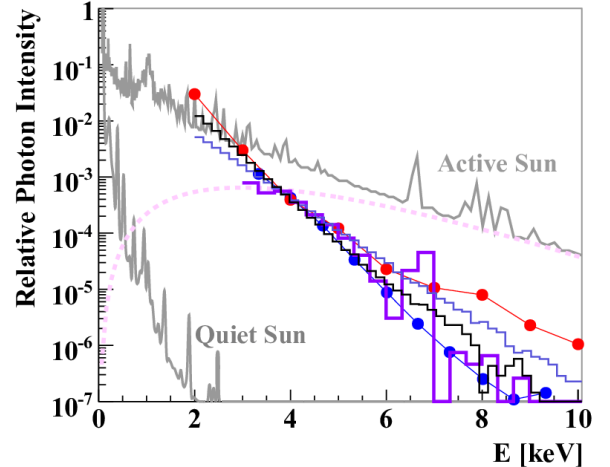


Figure 2: Solar X-ray spectrum

Due to limited XSM data as compared to CLASS data, we fitted the power law to model the XSM continuum over all processed XRF files. The Power law model was fitted by removing peaks and fitting the continuum over the remaining spectrum. This continuum will represent Solar spectra directly incident on the detector and the one which was reflected back and then detected on the detector and is used to subtract and then divide the processed XRF spectra [Zioutas et al. \(2010\)](#).

### 3.7. Elemental ratio Mapping

Elements abundances are analyzed relative to Si since it is the most abundant element in the lunar crust. In Apollo 15 and 16 experiments the abundance of Si was considered to be invariant throughout the lunar surface and Al/Si and Mg/Si ratios were estimated. This approach demands a precise knowledge of the reference element and yields only relative abundances. Si is considered a general basis for determining elemental ratios. This gives us insights into elemental composition. We determined Mg/Si, Al/Si, Ca/Si, Ti/Si, Cr/Si, and Fe/Si ratios corresponding to detected positive peaks of these elements with respect to detected peaks of Si. Ratios were calculated by dividing the peak intensities of elements. Ratios can not be calculated where either of the elements' signifying ratios was not detected. These ratios majorly lie in the range of 0-1. There were fewer files with a ratio value of more than 1 and some were outliers. Ratios were plotted on the LROC

map according to location coordinates with each ratio file represented as a patch of  $12.5\text{km} \times 12.5\text{km}$  with a color gradient corresponding to the ratio value Athiray et al. (2013).

### 3.8. Compositional group analysis

Lunar crustal terrain is divided into various geological features. Studies from the Lunar Prospector gamma-ray mission (1998-1999) suggests that the lunar crust and underlying mantle has been divided into distinct terranes that possess unique geochemical, geophysical, and geological characteristics. Lunar geomorphology contains basaltic maria, feldspathic Highland, and impact basins. Each feature contains unique morphology and distinct chemical characteristics. These can be studied through elemental composition maps. In our research interest Major features; Mara, Highland, and The South Pole impact basin were analyzed depending on major elemental ratios with respect to Si and features showed distinct characteristics Jaumann et al. (2012).

### 3.9. Defining best ratios for visualization

Elemental ratios are calculated to study the morphology and composition of different lunar structures. It is important to define ratios of significance for our research. Significance of ratio for analysis depends on various factors like coverage, uncertainty in ratio values at particular locations during different observations which defines the reliability of ratios, and heterogeneity in ratio maps which show compositional variation in different lunar structures. Ratios having higher coverage allow us to do analysis even in smaller regions. Ratios of lighter or abundant elements; with respect to Si give higher coverage due to significant excitation for XRF. Uncertainty was calculated using the Standard error of the mean; lower the uncertainty, the higher is the reliability of ratios. The ratios having variation while navigating to different lunar structures allows us to draw insights about the chemical composition and morphology of structures. Ratios varying independently of geological structures are of less significance for analysis but could potentially open new areas of research about their variation. Considering these factors best ratios can be defined as having significant coverage and abundance, lower uncertainty, and geological variation for global analysis. Elements having globally less abundance are concentrated over certain lunar structures, for in-situ analysis these elemental ratios can also serve as best ratios.

### 3.10. Improving Sub-pixel Resolution

The maximum pixel resolution we can achieve for CLASS data corresponds to  $12.5\text{km} \times 12.5\text{km}$  per file which gives us overall information of a particular location at this scale. Using multiple observations over a certain region from overlapping observation patches in consecutive observations or the observation taken of that area during different revolution orbits we can recalculate ratios for overlapping areas as the mean of ratios from overlapping observations. This is done to reduce complexity as we have limited information about location-specific geological parameters affecting transition in ratios at consecutive observations and limited information about instrumental uncertainties due to the change in flare activity in the case of overlapping caused by observation taken over that area in a different revolution orbit of Chandrayaan 2. This will not give us actual information about specific overlapping regions but is a precise estimate to visualize ratios at increased resolution.

## 4. Results and Analysis

### 4.1. Elemental ratio maps

Lunar structures depicted distinct elemental compositional characteristics in ratio maps setting a dais to study evolution dynamics, to understand geological and geochemical phenomena occurring on the lunar surface. O, Mg, Al, Si, and Fe showed significant coverage as is evident from past missions. Mg, Al, and Si showed significant peak detections followed by O and Fe. Elemental ratio maps relative to Si exhibited a strong correlation with geological features and can clearly distinguish between major geological structures such as Highland, Maria, Impact basins, and major craters. On further experimentation, ratios with respect to O also exhibited a strong correlation with geological features. Box plots were analyzed to study the distribution of ratio values over the range.

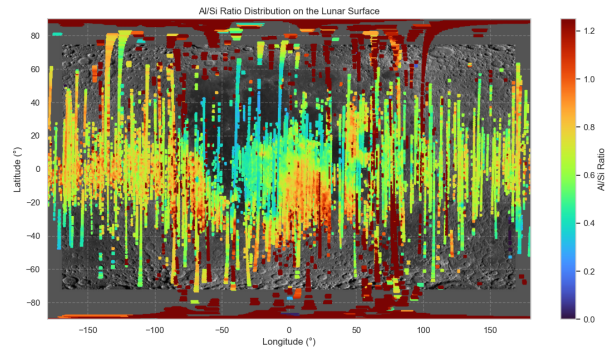


Figure 3: Al/Si ratio map

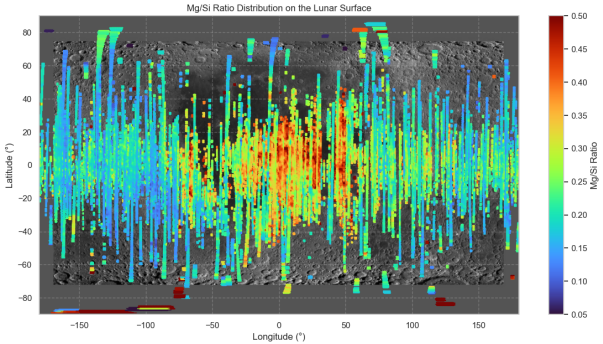


Figure 4: Mg/Si ratio map

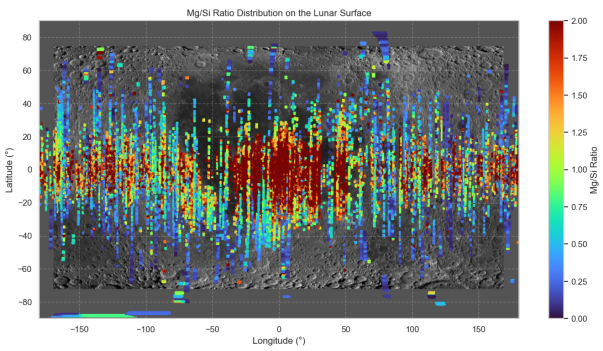


Figure 5: O/Si ratio map

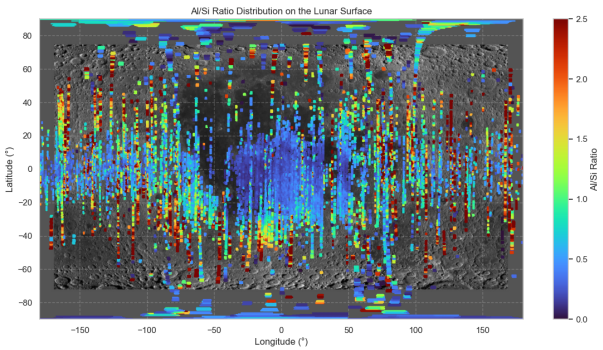


Figure 6: Al/O ratio map

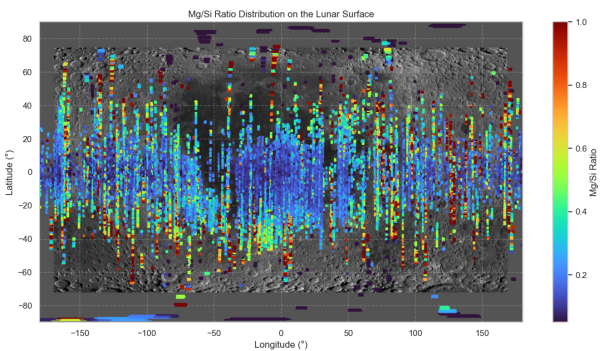


Figure 7: Mg/O ratio map

#### 4.2. Deriving uncertainties and defining best ratios

Uncertainties were derived from overlapping tracks. The percentage standard mean error was calculated for each ratio by leveraging regions having multiple observations with overlap over the particular area. This provided us with a statistical value of uncertainty of our instrument's measurement over a particular region at different observations, corresponding to different times and flare activities. Uncertainty was not defined for the areas having a single CLASS observation. The more precise method is to find systematic uncertainty but due to limited information about the characteristic parameters of instruments normal certainty was taken as a measure to define uncertainty in overlapping tracks.

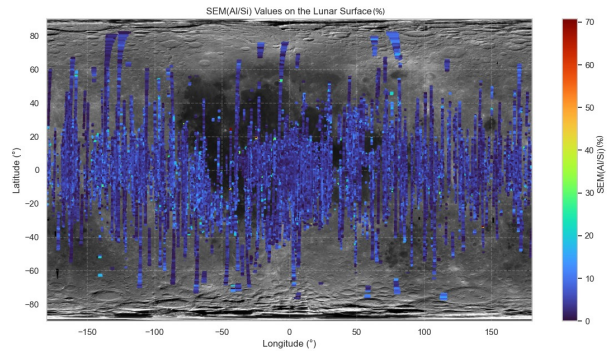


Figure 8: Al/Si ratio uncertainty map

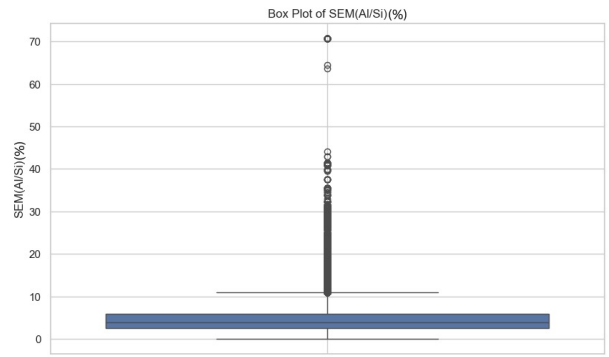


Figure 9: Al/Si ratio uncertainty map

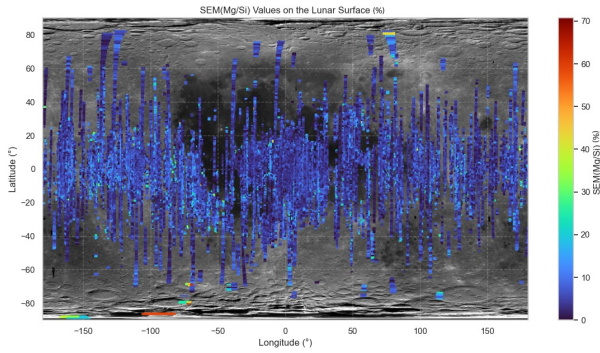


Figure 10: Mg/Si ratio uncertainty map

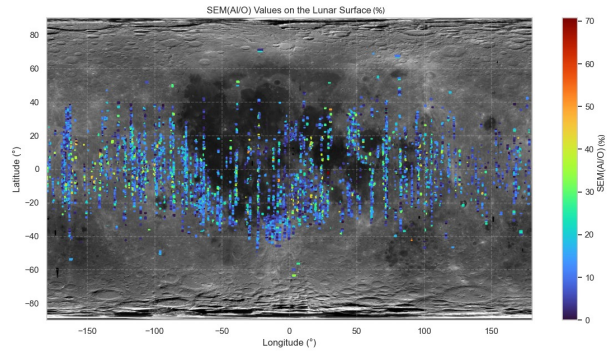


Figure 14: Al/O ratio uncertainty map

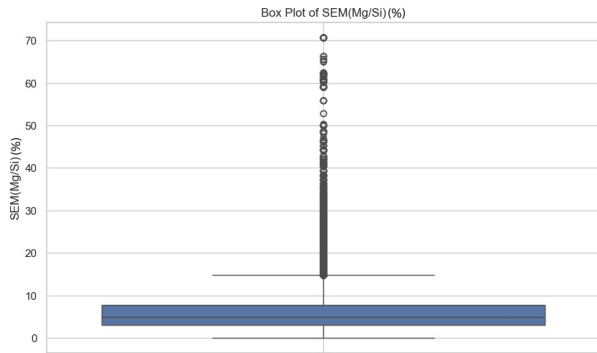


Figure 11: Mg/Si ratio uncertainty map

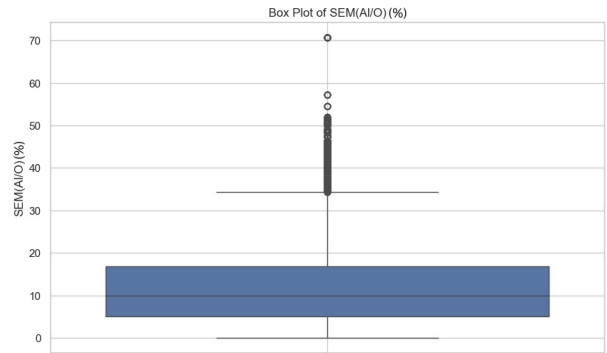


Figure 15: Al/O ratio uncertainty map

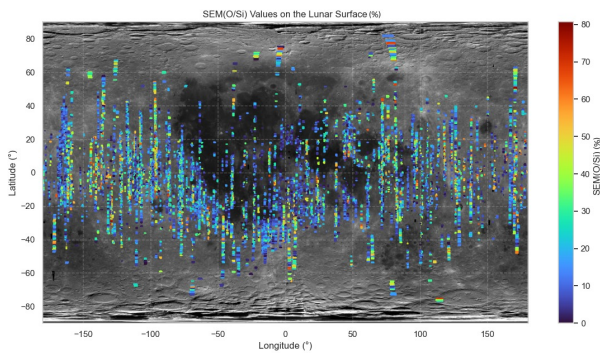


Figure 12: O/Si ratio uncertainty map

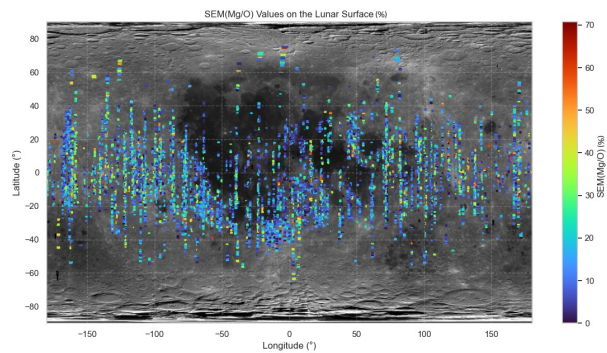


Figure 16: Mg/O ratio uncertainty map

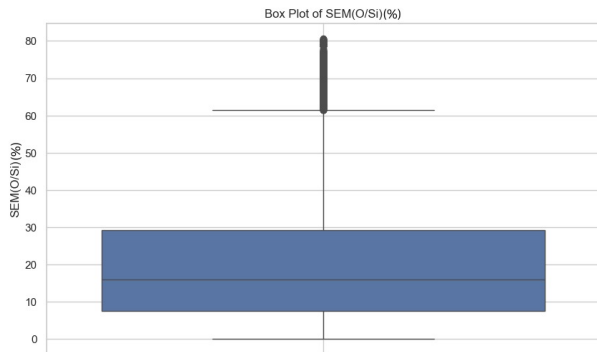


Figure 13: O/Si ratio uncertainty map

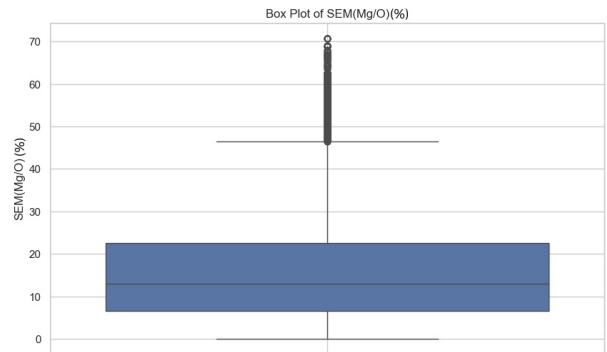


Figure 17: Mg/O ratio uncertainty map

Uncertainty of Mg/Si and Al/Si were comparatively less with most of the uncertainties having value around 5%. For further analysis, we studied O/Si and other ratios with respect to O but uncertainty values surged for these ratios. This is due to the non-precise detection of Oxygen peaks at lower energy of excitation. Having  $K\alpha$  excitation of 0.53 eV makes detection difficult leading to less precise peak detection as compared to other elements. Moreover, heterogeneity of ratio behavior across different lunar features was seen in ratios of all major elements. Thus lower uncertainties of Mg/Si and Al/Si with high coverage, qualify them to be the best ratios from calculated ratios. These ratio maps with low uncertainty, implying better consistency of CLASS detection can be studied further to draw insights about geochemical composition on finer scales.

### Studying features and compositional groups

Conducting analysis for ratios of Mg/Si and Al/Si we are able to study ratio variation across lunar features. Mare basalts consist of Al/Si ratios around the range of 0.2 to 0.4 whereas Mg/Si was found around the range of 0.3 to 0.5 and higher. In Highland, the Al/Si ratio lies around the range of 0.6 to 1.2 and higher whereas Mg/Si lies around the range of 0.1 to 0.2. The major chunk of data lies around these ratio ranges but variation on a finer scale opens the door for studying features in regions on a finer scale.

### Finer Analysis

**Copernicus crater:** With a diameter of 93 km, the Copernicus crater stays highlighted on the lunar map with its significant elemental ratio variations from surrounding regions. The extreme surge in Mg/Si (more than 0.6) and Al/Si (greater than 1 ) ratio near the center signifies high Mg and Al concentration in magma. The finer boundary with the surge in ratio values near the center signifies a relatively young crater.

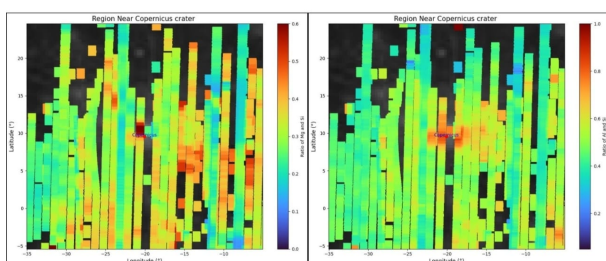


Figure 18: Mg/Si and Al/Si around Copernicus crater

### Validation of Results

Lunar samples provide us with ground truth information about elemental abundances which help us in calculating exact elemental ratios to validate the accuracy of our algorithm to calculate Elemental ratios. Analysis was conducted to validate results by comparing it to data from lunar samples and comparing it to results of C1XS and CLASS analysis. [Pillai et al. \(2021\)](#). Ratios were calculated using elemental abundances of C1XS and CLASS to compare the results from our algorithm.

Results exhibited a significant correlation with C1XS and CLASS analysis done previously. This can be seen in the [Table](#) shown in the next page

Scatter plots for the ratio of Al/Si showed a positive correlation for LPGRS and CLASS data. The Mg/Si ratio showed a weaker correlation for LPGRS and CLASS data.

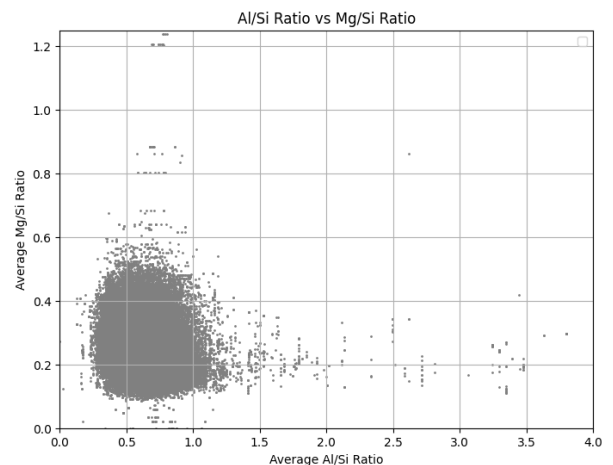


Figure 19: Al/Si Ratio vs Mg/Si Ratio

Scatter plots for the Al/Si ratio and Mg/Si ratio showed a negative correlation. This validates the inverse correlation of these ratios over the Mare and Highland regions.

### Comparision between LPGRS and our Results

We conducted a comparison test between LPGRS (Lunar Prospector Gamma Ray Spectrometer) (60km by 60km resolution) and our data (12.5km by 12.5km). First, we matched the resolution of the LPGRS's data by taking the smaller overlapping (greater than 90%) grids of the calculated CLASS data and averaging the ratios. Thereafter scatter plots for these ratios between the two datasets are plotted and shown here. Datasets for LPGRS were taken from this website: [LPGRS](#)

| Data                | Coordinates   | Mg/Si          | Al/Si         | Mg/Al         |
|---------------------|---|----------------|---------------|---------------|
| C1XS                | (-30.2, 25)   | 0.272±0.070    | 1.04 ± 0.12   | 0.260 ± 0.076 |
| CLASS-1             | (-30.2, 25)   | 0.279 ± 0.371  | 0.804 ± 0.323 | 0.346 ± 0.378 |
| CLASS (our results) | (-31.6021, 25.9409),<br>(-32.8305, 24.9455),<br>(-32.8432, 25.9238),<br>(-31.6146, 25.9409) | 0.264 ± 0.022  | 0.819 ± 0.064 | 0.32±0.016    |
| C1XS                | (6.92, -17.34)  |                |               | 0.57 ± 0.26   |
| CLASS               | (6.92, -17.34)  |                |               | 0.593±0.422   |
| CLASS (our results) | (7.6357, -16.1659),<br>(6.2424, -17.2018),<br>(6.2208, -16.1998),<br>(7.6319, -16.1659)     | 0.316 ± 0.0069 | 0.597 ± 0.005 | 0.52 ± 0.015  |
| 15012               | (26.06, 3.65)   | 0.331          | 0.422         | 0.785         |
| CLASS-1             | (26.06, 3.65)   | 0.343±0.124    | 0.504±0.222   | 0.681±0.303   |
| CLASS (our results) | (26.2618, 4.1512),<br>(25.0005, 3.1652),<br>(24.9797, 4.1108),<br>(26.2407, 4.1512)         | 0.4028±0.027   | 0.6691±0.064  | 0.6019±0.0217 |

Table 1: Comparison between location-specific elemental ratios from C1XS, Apollo samples, CLASS, and our results

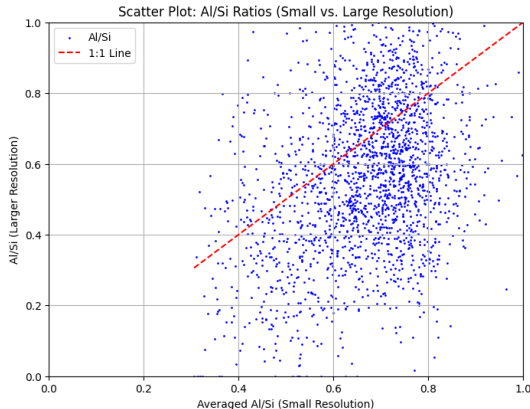


Figure 20: Scatter Plot between LPGRS and CLASS data for Al/Si Ratio

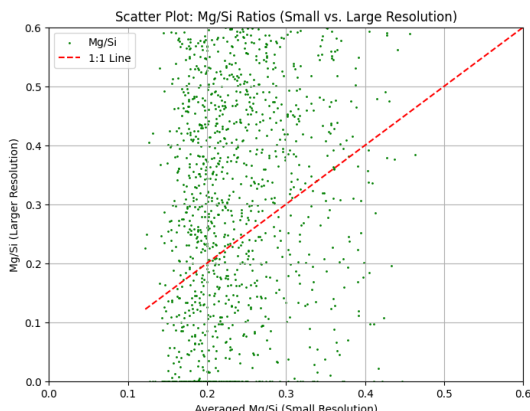


Figure 21: Scatter Plot between LPGRS and CLASS data for Mg/Si Ratio

## Further Analysis

**Magnesium number (Mg#)** - To leverage the high coverage and low uncertainties of ratios, we conducted an analysis for magnesium number (Mol % of Mg / (Mg + Fe), Mg#) to draw insights about volcanic activities in the past over the lunar surface, it provides a degree of differentiation of the magma ocean at the time of its solidification. Mg# is used to discuss the origin of dichotomy and determine the Lunar Magma Ocean's cooling history [Otake et al. \(2012\)](#).

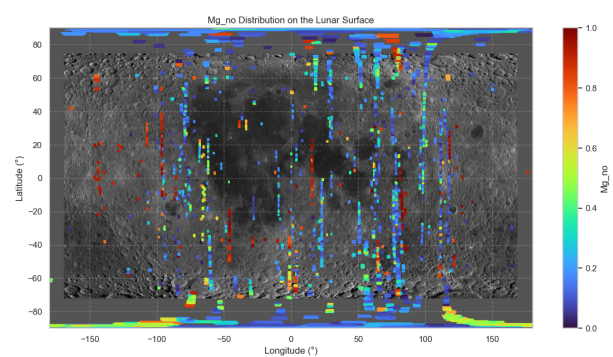


Figure 22: Mg# map

Lunar Near side, containing Mare basaltic region have lower Mg# compared to high Mg# in far side containing Highland. The most extensive high-Mg# region is at the center of the feldspathic highland terrain. Higher Mg# implies crystallization from a less evolved magma ocean.

lower Mg# on lunar near side compared to lunar far side suggests that lunar near side is less magma evolved than of far side. This mare basaltic region with low Mg# suggests crystallization from more recent and extensive volcanism. Far side Highland have been crystallized comparatively earlier and from highly evolved magma oceans owing to its high Mg#. This analysis is presently conducted on limited lunar coverage of high resolution Mg and Fe and can be further extended in detailed research to study lunar volcanism in different regions in the past through high resolution and extensive lunar coverage data of Mg and Fe from upcoming observations.

## 5. Conclusion

Global coverage of elemental composition with better accuracy is important to study lunar evolution. CLASS provided the highest coverage of lunar XRF data with a maximum spatial resolution of  $12.5\text{km} \times 12.5\text{km}$  compared to previous missions. Location-specific information from CLASS XRF helped detailed analysis of elemental composition. The most extensive dataset of CLASS over its projected lifespan of 7 years will give data in fine corners of the lunar surface. A clear distinction between several lunar features through resolution-improved lunar elemental ratio maps helps us in the finer analysis of regions to study chemical composition and mineralogy. Understanding lunar mineralogy and potential resources in fine cores can support for utilization of those resources for high energy requirements of future deep space and interplanetary exploration missions of mankind. With the upcoming 2 years of data from CLASS XRF and additional exploration by Chandrayaan 3, we would get enhanced information about the lunar surface and its characteristics.

## References

- Athiray, P., Narendranath, S., Sreekumar, P., Dash, S. and Babu, B. (2013), 'Validation of methodology to derive elemental abundances from x-ray observations on chandrayaan-1', *Planetary and Space Science* **75**, 188–194.
- Ban, C., Zheng, Y., Zhu, Y., Zhang, F., Xu, L. and Zou, Y. (2014), 'Research on the inversion of elemental abundances from chang'e-2 x-ray spectrometry data', *Chinese Journal of Geochemistry* **33**, 289–299.
- Gloudemans, A. J., Kuulkers, E., Campana, R., Escalante, A., Kole, M. and Mollard, Y. (2021), 'Re-evaluation of lunar x-ray observations by apollo 15 and 16', *Astronomy & Astrophysics* **649**, A174.
- Ito, Y., Tochio, T., Yamashita, M., Fukushima, S., Shoji, T., Slabkowska, K., Syrocki, Ł., Polasik, M., Gomilsek, J. P., Marques, J. P. et al. (2023), 'Intensity ratio of  $\text{k}\beta/\text{k}\alpha$  in selected elements from mg to cu, and the chemical effects of cr  $\text{k}\alpha$  1, 2 diagram lines and cr  $\text{k}\beta/\text{k}\alpha$  intensity ratio in cr compounds', *International Journal of Molecular Sciences* **24**(6), 5570.
- Jaumann, R., Hiesinger, H., Anand, M., Crawford, I., Wagner, R., Sohl, F., Jolliff, B., Scholten, F., Knapmeyer, M., Hoffmann, H. et al. (2012), 'Geology, geochemistry, and geophysics of the moon: Status of current understanding', *Planetary and Space Science* **74**(1), 15–41.
- Narendranath, S., Athiray, P., Sreekumar, P., Kellett, B., Alha, L., Howe, C., Joy, K., Grande, M., Huovelin, J., Crawford, I. et al. (2011), 'Lunar x-ray fluorescence observations by the chandrayaan-1 x-ray spectrometer (c1xs): Results from the nearside southern highlands', *Icarus* **214**(1), 53–66.
- Nishida, A., Uesugi, K., Nakatani, I., Mukai, T., Fairfield, D. and Acuña, M. (1992), 'Geotail mission to explore earth's magnetotail', *Eos, Transactions American Geophysical Union* **73**.
- Ohtake, M., Takeda, H., Matsunaga, T., Yokota, Y., Haruyama, J., Morota, T., Yamamoto, S., Ogawa, Y., Hiroi, T., Karouji, Y. et al. (2012), 'Asymmetric crustal growth on the moon indicated by primitive farside highland materials', *Nature Geoscience* **5**(6), 384–388.
- Okada, T., Shirai, K., Yamamoto, Y., Arai, T., Ogawa, K., Shiraishi, H., Iwasaki, M., Kawamura, T., Morito, H., Grande, M. and Kato, M. (2010), 'X-ray fluorescence spectrometry of lunar surface by xrs onboard selene (kaguya)', *Transactions of The Japan Society for Aeronautical and Space Sciences, Space Technology Japan* **7**.
- Pillai, N. S., Narendranath, S., Vadodariya, K., Tadepalli, S. P., Radhakrishna, V., Tyagi, A., Yadav, R., Singh, B., Sharan, V., Athiray, P. et al. (2021), 'Chandrayaan-2 large area soft x-ray spectrometer (class): calibration, in-flight performance and first results', *Icarus* **363**, 114436.
- Swinyard, B., Joy, K., Kellett, B., Crawford, I., Grande, M., Howe, C., Fernandes, V., Gasnault, O., Lawrence, D., Russell, S. et al. (2009), 'X-ray fluorescence observations of the moon by smart-1/d-cixs and the first detection of  $\text{Ti}\text{k}\alpha$  from the lunar surface', *Planetary and Space Science* **57**(7), 744–750.
- Zioutas, K., Tsagri, M., Semertzidis, Y., Papaevangelou, T., Gardikis, A., Dafni, T. and Anastassopoulos, V. (2010), 'Solar x-rays from axions: Rest-mass dependent signatures', *Proceedings of the 5th Patras Workshop on Axions, WIMPs and WISPs, PATRAS 2009*.